

Taming nuclear complexity with a committee of deep neural networks

David Regnier**

*Centre de mathématiques et de leurs applications, CNRS,
ENS Paris-Saclay, Université Paris-Saclay, 94235, Cachan cedex, France*

Raphaël Lasserri*†

ESNT, CEA, IRFU, Département de Physique Nucléaire, Université Paris-Saclay, F-91191 Gif-sur-Yvette

Jean-Paul Ebran‡

CEA, DAM, DIF, F-91297 Arpajon, France

Antonin Penon§

Magic LEMP, 2 Rue Jean Rostand, 91400 Orsay, France

We demonstrate that a committee of deep neural networks is capable of predicting the ground-state and excited energies of more than 1800 atomic nuclei with an accuracy akin to the one achieved by state-of-the-art nuclear energy density functionals (EDFs) and a major speed-up. An active learning strategy is proposed to train this algorithm with a minimal set of 210 nuclei. This approach enables future fast studies of the influence of EDFs parametrizations on structure properties over the whole nuclear chart and suggests that for the first time an artificial intelligence successfully encoded the laws of nuclear deformation.

Keywords: Artificial Intelligence, Machine Learning, Nuclear Structure, Energy Density Functional, Beyond Mean Field, Active Learning

Introduction Today, more than 3000 atomic nuclei were identified, revealing the wide diversity of nuclear phenomenology (deformation, superfluidity, clustering, halo, ...). Predicting nuclear properties over the whole range of known mass and charge and beyond is therefore a daunting challenge yet essential to unveil new exotic states of matter, foster our quest to the super heavy island of stability and answer the fundamental questions of nucleosynthesis. Among the different microscopic approaches of nuclear structure, only the framework of energy density functionals (EDFs) [1] is currently capable of providing a complete and accurate description of ground- and excited-state properties [2–4]. Large-scale deployment of nuclear EDFs is however associated with a high computational cost, especially when it is implemented at its multireference level (MR-EDFs), also referred as beyond mean field. Such a cost hurdles our understanding of the variations of global nuclear features with different EDFs. Ultimately, fitting an effective interaction at the beyond mean field level is a tremendous task that was only undertaken once [5] and yielded a root mean square error (RMS) on the experimentally known masses of 790 keV. As a result most of our beyond mean field calculations are based on EDFs fitted at the mean field level which brings a double counting bias in the predictions. Attacking the problem from a different angle, Athanasopoulos *et. al.* built a neural network capable of predicting the whole nuclear table of mass with a RMS of 950 keV [6]. This idea has then been further explored by training neural networks, bayesian networks or gaussian processes to predict the residual between an existing theory and experimental data. It was applied on different

models and observables (masses, charge radii and two neutron separation energies) and reduces typically the binding energy RMS to a few hundreds of keV [7–13]. In all these studies, the quality of the predictions is obtained (i) by the knowledge of an initial model with good performances (typically 1-2 MeV RMS on the ground state mass), (ii) by training the artificial intelligence (AI) on a vast amount of experimental data (especially masses and radii), typically 80% of one of the Atomic Mass Evaluations (AME) [14] i.e. more than 1800 nuclei. This large training set, as well as the fact that the AI can only predict one observable, severely restricts the predictive capability of such fast approaches as compared to the EDF approach. In this letter, we propose a new strategy where an AI learns not one observable but several intermediate quantities (potential energy surfaces and inertia) involved in a multireference EDF approach. The idea is that while speeding up drastically the calculation of these quantities, the AI will get a rich understanding of the underlying physics of nuclear deformation by learning several of its aspects simultaneously. After a training step, this approach also enables to compute from the AI's predictions multiple low-energy observables such as the ground state and excited energies.

Method In this work, nuclear structure properties are tackled within the five-dimensional collective Hamiltonian (5DCH) approach [15–18]. First, constrained Hartree-Fock-Bogoliubov (HFB) calculations in the collective space spanned by both the axial and triaxial quadrupole mass moments capture the static correlations associated to quadrupole deformation and pairing. The generation of the manifold of constrained HFB so-

lutions, labeled by the quadrupole deformation variables (β, γ) , is by far the most demanding in terms of numerical resource. Then, the effect of the quantum-mechanical fluctuations of the order parameters β and γ around the minimal energy region is accounted for through the construction and solving of the 5DCH. More precisely, from the HFB constrained states and the corresponding potential energy surface $E_{\text{HFB}}(\beta, \gamma)$, the 2×2 symmetric matrix $\mathbf{B}(\beta, \gamma)$ that stands for the collective vibrational inertia, the rotational inertia $\mathcal{I}_k(\beta, \gamma)$ associated to the three axis k of the intrinsic frame, and the zero-point energy correction $\Delta V(\beta, \gamma)$ are computed and yield the collective eigenproblem

$$\left(\hat{\mathcal{H}}_{K,rot} + \hat{\mathcal{H}}_{K,vib} + \hat{\mathcal{H}}_V \right) g_i(\beta, \gamma, \mathbf{\Omega}) = E_i g_i(\beta, \gamma, \mathbf{\Omega}). \quad (1)$$

The functions $g_i(\beta, \gamma, \mathbf{\Omega})$ are the unknown collective wave functions of the nucleus. The collective Hamiltonian contains (i) a kinetic term $\hat{\mathcal{H}}_{K,rot}$ associated to rotation that couples the quadrupolar degrees of freedom to the Euler angles $\mathbf{\Omega}$, (ii) a vibrational kinetic term $\hat{\mathcal{H}}_{K,vib}$ containing the second derivatives of the collective wave functions with respect to β and γ , (iii) a potential term $\hat{\mathcal{H}}_V$ that only depends on the quadrupolar deformations and contains the HFB energy shifted by the zero-point energy correction. The eigensolutions of Eq. (1) directly yield the correlated ground state energy as well as the typical rotational and vibrational bands of the excitation spectrum.

The main idea of this work is to simultaneously teach the eight collective functions $E_{\text{HFB}}, \Delta V, \mathbf{B}_{00}, \mathbf{B}_{01}, \mathbf{B}_{11}$ and \mathcal{I}_k ($k = 1, 2, 3$) defining the collective Hamiltonian to an AI to make it learn the physics of nuclear deformation. Our AI consists of a committee of feed forward deep neural networks [19] that undertake the regression of these functions. Each neural network takes as input the number of neutrons N and protons Z and returns the values of the eight functions on a discretized mesh of the deformation space. After a learning stage involving a random initialization of each member, the prediction of the committee is obtained by averaging the outputs of its members. The benefit of using a committee is twofold: (i) reducing the variance of the prediction associated to the random initialization of the members, (ii) providing a simple estimation of this variance which we can leverage in an active learning procedure.

The members of the committee all have the same network architecture. Their input is the number of neutrons and protons encoded in 600 bits string as detailed in Ref. [20]. Note that contrary to Ref. [11], we chose an encoding that is totally agnostic of any *a priori* knowledge of the physics (*i.e.* shell effects) to avoid biasing the AI's predictions in the exotic areas of the nuclear chart. Internally, the neural networks contain five hidden layers defined by the sequence 600 – 300 – 150 – 100 – 75 of their number of neurons. The first part of the net-

work embeds the information of the nucleus into a neck of 75 neurons only while its second part predicts from this embedding the output functions. We attempted to fine-tune some hyper-parameters of this architecture such as the number, size and types (dense, convolutions, etc) of the hidden layers with a grid-search approach. This turned out not to modify significantly the results that we present here.

With this choice of architecture, we perform a supervised training on a set of nuclei for which we know the collective functions from previous constrained HFB calculations. To maximize the quality of the AI while minimizing the number of HFB calculations required we implemented an active learning procedure inspired by Ref. [21]. It consists of an iterative algorithm which can be summarized by these few steps:

1. Sample an initial training set of nuclei and compute their collective functions with constrained HFB.
2. Train each member of the committee on this set.
3. Query from the committee a set of additional nuclei that are likely to improve the predictions of the AI if added in the next training step.
4. Compute the collective functions of these new nuclei with constrained HFB and add them into the training set.
5. Re-iterate from step 2 up to some stopping criteria.

At step 2, we train independently the neural networks corresponding to each member of the committee following a standard technique in machine learning. This procedure, detailed in Refs [20, 22–25], minimizes a training loss while avoiding overfitting the network. The training loss consists on a weighted sum of the partial losses $\mathcal{L}_t(N, Z)$ per nucleus (N, Z) and per output function t . The partial losses are themselves defined as the squared error between the AI's prediction t_{AI} and the HFB calculation t_{HFB} averaged on the deformation space $(\beta, \gamma) \in [0, B = 0.9] \times [0, \frac{\pi}{3}]$ for one nucleus:

$$\mathcal{L}_t(N, Z) = \frac{6}{\pi B^2} \int_{\beta, \gamma} |t_{\text{AI}}(\beta, \gamma) - t_{\text{HFB}}(\beta, \gamma)|^2 d\beta d\gamma. \quad (2)$$

After each training stage, five new nuclei are added to the training set. To select them, we improved the method proposed in Ref. [21] in the following way. Each member of the committee makes a prediction for more than 2000 nuclei and we first isolate the 10% for which the standard deviation between members is the highest. Then we use a k-means algorithm to detect five clusters among these nuclei and take in each cluster the nucleus for which members predictions differ the most. To accelerate the training process, we normalized each output function (cf. [20]). The HFB energy is for instance transformed by

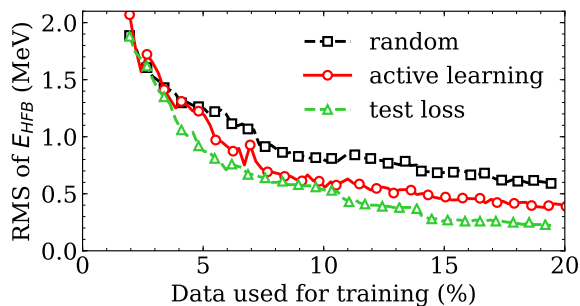


FIG. 1: RMS of the HFB energy on the test nuclei as a function of the size of the training set (in percent of the AMEDEE database). We compare results obtained with a training set determined by the active learning (red), by random sampling (black) and by an incremental choice based on the test loss (green).

first removing a deformed liquid drop formula inspired from Ref. [26] and then performing a linear scaling so to obtain a zero mean and unity standard deviation on the training set of nuclei.

Results We consider a data set of 2100 even even nuclei taken from the AMEDEE database [27] and with the charge and neutron ranges $Z \in [10, 120]$ and $N \in [10, 260]$. For these nuclei, we dispose of the eight functions $E_{\text{HFB}}, \Delta V, \mathbf{B}_{00}, \mathbf{B}_{01}, \mathbf{B}_{11}$ and \mathcal{I}_k ($k = 1, 2, 3$) calculated at 94 deformation points with the Gogny D1S effective interaction [28]. For each nucleus, we first interpolated these raw data on a 64×64 regular grid with splines of degree two. We start the active learning of the AI with 2% of the nuclei sampled randomly from an adapted latin hyper cube sampling approach, that ensures a certain uniformity in the N, Z plan. We then run the active learning up to a training set containing 20% of the 2100 nuclei. At each learning step, we evaluate the quality of the AI's predictions on the M_{test} test nuclei not present in the training set ($M_{\text{test}} > 80\%$ of the database). To do so we determine for each output function t its associated RMS defined as:

$$\text{RMS}(t) = \left(\frac{1}{M_{\text{test}}} \sum_i^{M_{\text{test}}} \mathcal{L}_t(N_i, Z_i) \right)^{1/2} \quad (3)$$

We show in Fig. 1 the evolution of the RMS associated to the HFB energy as a function of the size of the training set. Starting above 2 MeV, it follows an exponential like decrease to reach less than 400 keV at 20%. We compare these results with the ones obtained if we train the same AI on a set of nuclei that is (i) randomly chosen at each step (ii) incremented at each step with the 5 nuclei that maximize the global test loss (computed on the test set). Note that this last procedure requires the a priori knowledge of the HFB results for all nuclei. The active learning outperforms the naïve random training set by roughly 200 keV for training set sizes in between

Training %	E_{HFB} (keV)	ΔV (keV)	\mathcal{I}_1 ($\hbar^2 \times \text{MeV}^{-1}$)	\mathcal{I}_2 ($\hbar^2 \times \text{MeV}^{-1}$)	\mathcal{I}_3 ($\hbar^2 \times \text{MeV}^{-1}$)	\mathbf{B}_{00} (MeV^{-1})	\mathbf{B}_{01} (MeV^{-1})	\mathbf{B}_{11} (MeV^{-1})	E_{GS} (keV)
5	1190	417	1.84	2.80	0.97	13.8	12.0	28.2	1325
10	557	312	1.40	2.25	0.76	11.7	10.2	23.9	716
15	471	247	1.25	2.02	0.69	10.6	9.4	21.9	655
20	388	202	1.22	1.96	0.68	10.2	9.1	21.2	518

TABLE I: RMS obtained on the test set at different stages of the active learning. The first column contains the size of the training set in % of the AMEDEE database while the others highlight the RMS of the outputs of the AI. The last column contains the RMS associated to the correlated ground state energy E_{GS} solution of Eq. (1).

10% and 20%. In addition, the training based on the test loss gives even better results in this region. This shows the possibility that a more sophisticated algorithm of active learning could still improve our current results. Choosing the size of the training set is a tradeoff between the accuracy of the resulting AI and the numerical cost spent in the HFB calculations for the training nuclei. In Tab. I, we report the RMS of the eight output functions obtained at four different steps of the active learning. A striking result is the quality of the AI's prediction already achieved with only 10% of the total dataset. The HFB energy, which is a key feature in the determination of the correlated energies, is reproduced within 557 keV over the 1890 nuclei of the test set. In the following we therefore show the results obtained with this 10% training set.

The quality of the AI's prediction varies with N and Z . To assess what parts of the nuclear chart are correctly grasped by the AI, we emphasize in Fig. 2 the individual RMS per nucleus $\mathcal{L}_t^{1/2}(N, Z)$ for three different kinds of outputs. For the HFB energy, the AI captures very well the vast majority of heavy nuclei but struggles in the medium and light sectors ($N < 50$). A specially high RMS is found close to the $N = Z$ line where HFB calculations are known to predict an energy cusp often corrected in mass fits with the so called Wigner energy (see Ref. [29, 30]). The difficulty to reproduce the HFB energies in the light sector with an AI was already encountered in Ref. [11] and is related to the sharp variations present in this region. The panel (a) of Fig. 2 shows that the active learning procedure automatically densified the training set in this region to mitigate this difficulty. Concerning the vibrational and rotational inertia the error of the AI globally increases with the mass and some of the error peaks can be identified close to shell closures, e.g. for the vibrational inertia close to the neutron number $N = 80$. We compare in Fig. 3 the AI and reference HFB predictions of three collective functions for ^{178}Os . We choose this nucleus because (i) its excitation spectrum is known experimentally and (ii) its AI to reference calculation $\text{RMS}(E_{\text{HFB}}) = 409$ keV lies just above the median RMS over the test set. It is there-

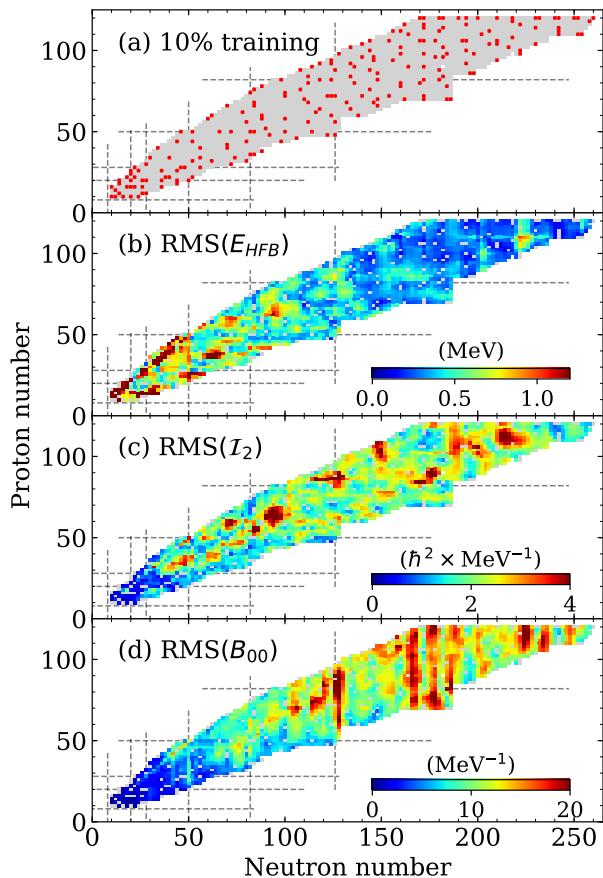


FIG. 2: (a) The AME2003 database nuclei are plotted in grey as a function of N and Z . The red squares stand for nuclei included in the 10% training set obtained by the active learning. The panels (b),(c) and (d) display the resulting RMS per nucleus ($\mathcal{L}_t^{1/2}(N, Z)$) for the three outputs E_{HFB} , \mathcal{I}_2 and \mathcal{B}_{00} respectively.

fore representative of how the AI performs for most of the test nuclei. Once again, the overall topology of E_{HFB} , \mathcal{I}_2 and \mathcal{B}_{00} are very well grasped by the AI despite the fact that the closest nucleus in the training set is the ^{180}W which has 4 additional neutrons and 2 protons less.

Finally we focus on the correlated ground state energy and excitation spectra obtained from Eq. (1). To solve the eigenproblem, we discretized the Euler angle space on the basis of Wigner rotational wave functions as in Ref. [15] whereas the deformation space is discretized on a finite element basis implemented with the FELIX-2.0 library [31]. We perform the comparison between the AI and HFB reference for 1666 nuclei of the test set for which the minimum of the potential energy lies below $\beta = 0.8$. This simple filter removes the super-heavy nuclei with an open fission channel in our deformation space, for which the ground state would be spuriously predicted at too high deformations. As reported in Tab. I, we obtain a RMS of 716 keV for the ground state energy, an accuracy

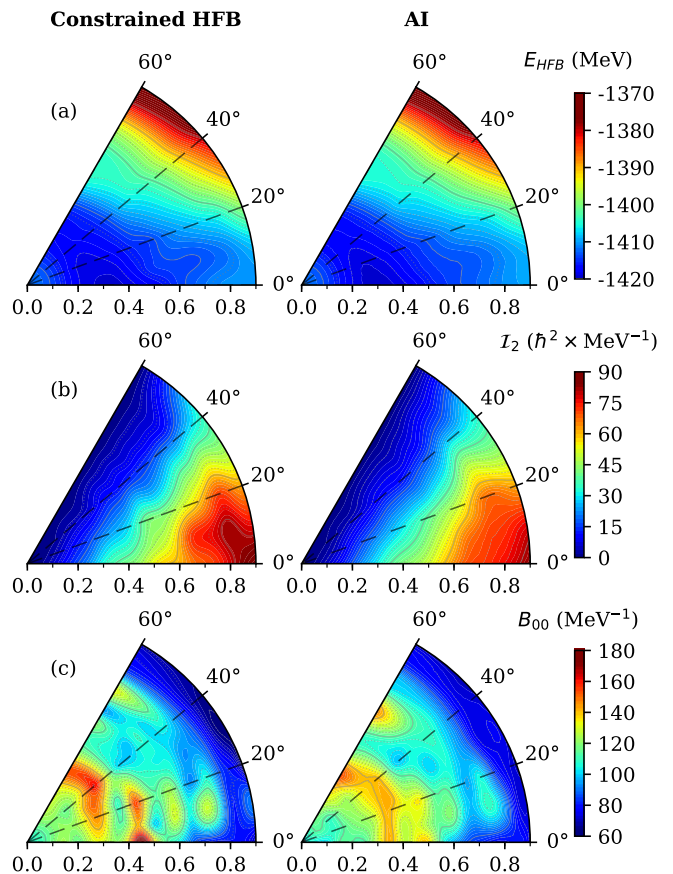


FIG. 3: HFB energy (a), rotational inertia along the principal axis (b) and vibrational inertia related to elongation (c) resulting from both constrained HFB calculations and the AI. These functions are plotted for ^{178}Os in the standard polar representation where β is the radial coordinate and γ the polar angle.

akin to the performance of state-of-the-art nuclear EDFs (500-800 KeV for the Skyrme HFB mass models [32, 33]). Fig. 4 displays the excitation spectra of ^{178}Os obtained from both the HFB and AI calculation and give for the sake of completeness the experimental values taken from the ENSDF database [34]. The rotational band predicted by the AI impressively matches the HFB data with only a 8% deviation for the first 2^+ , 4^+ and 6^+ states. Finally, the first excited 0^+ level is reproduced within 13% despite the complexity of the vibrational inertia topology.

Conclusions In this work we built for the first time an AI capable of estimating the low energy structure of all nuclei from a given EDF. Stunning performances are achieved, viz. a RMS of 716 KeV on the correlated ground state energy with respect to the MR-EDF calculation for a training on only ~ 200 nuclei, with room for further improvements, e.g. by (i) refining the selection of the training set of nuclei (cf. Fig. 1), (ii) exploring more involved active learning techniques such as negative correlation learning [35], or more sophisticated kinds of

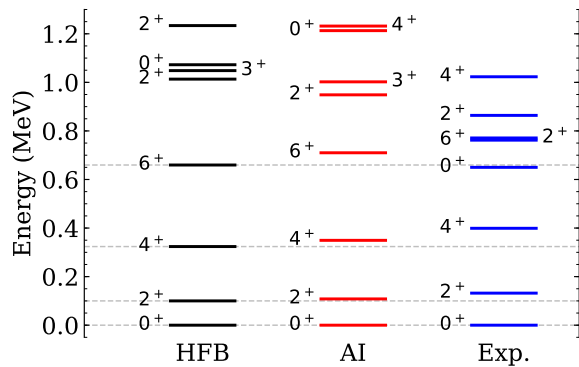


FIG. 4: Excitation spectrum of ^{178}Os obtained from both the AI (AI) and the constrained HFB calculations (HFB). The experimental spectrum (Exp.), taken from the ENSDF database [34], is also displayed.

neural networks. This fast framework opens the opportunity to quickly test the impact of new parametrizations of EDFs in the context of astrophysics and super-heavy production. On top of this, it paves the way toward fitting new EDFs at the MR level and with multiple observables (ground state masses, radii, and spectroscopic features). Finally, the success of this approach is a first proof of principle that an AI is able to encode the underlying physics of nuclear deformation. It implies that the AI possesses a satisfying non-trivial internal representation of the physics of the system. Studying this representation may unveil new physical concepts grasped by this AI.

The authors would like to thank J. Libert, S. Hilaire, G. Hupin and E. Kahn for fruitful discussions on the collective Hamiltonian and the nuclear mass tables, as well as N. Makaroff for his suggestion on activation functions. * D. Regnier and R. Lasserri contributed equally to this work.

* Electronic address: regnier@ipno.in2p3.fr

† Electronic address: raphael.lasserri@cea.fr

‡ Electronic address: jean-paul.ebran@cea.fr

§ Electronic address: penon@magic-lemp.com

- [1] N. Schunck, M. Bender, A. Bulgac, T. Duguet, J.-P. Ebran, J. Engel, M. F. Michael, M. Kortelainen, and T. Nakatsukasa, *Energy Density Functional Methods for Atomic Nuclei* (Institute of Physics Publishing, 2019).
- [2] M. Bender, *The European Physical Journal Special Topics* **156**, 217 (2008).
- [3] T. Nikšić, D. Vretenar, and P. Ring, *Progress in Particle and Nuclear Physics* **66**, 519 (2011).
- [4] J. L. Egido, *Phys. Scr.* **91**, 073003 (2016).
- [5] S. Goriely, S. Hilaire, M. Girod, and S. Péru, *Phys. Rev. Lett.* **102**, 242501 (2009).
- [6] S. Athanassopoulos, E. Mavrommatis, K. A. Gernoth, and J. W. Clark, *AIP Conference Proceedings* **831**, 397

- (2006).
- [7] R. Utama and J. Piekarewicz, *Phys. Rev. C* **96**, 044308 (2017).
- [8] H. F. Zhang, L. H. Wang, J. P. Yin, P. H. Chen, and H. F. Zhang, *J. Phys. G: Nucl. Part. Phys.* **44**, 045110 (2017).
- [9] R. Utama and J. Piekarewicz, *Phys. Rev. C* **97**, 014306 (2018).
- [10] L. Neufcourt, Y. Cao, W. Nazarewicz, and F. Viens, *Phys. Rev. C* **98**, 034318 (2018).
- [11] Z. M. Niu and H. Z. Liang, *Physics Letters B* **778**, 48 (2018).
- [12] S. Akkoyun, T. Bayram, S. O. Kara, and A. Sinan, *J. Phys. G: Nucl. Part. Phys.* **40**, 055106 (2013).
- [13] R. Utama, W.-C. Chen, and J. Piekarewicz, *J. Phys. G: Nucl. Part. Phys.* **43**, 114002 (2016).
- [14] M. Wang, G. Audi, F. G. Kondev, W. J. Huang, S. Naimi, and X. Xu, *Chinese Phys. C* **41**, 030003 (2017).
- [15] K. Kumar and M. Baranger, *Nuclear Physics A* **92**, 608 (1967).
- [16] J. Libert, M. Girod, and J.-P. Delaroche, *Phys. Rev. C* **60**, 054301 (1999).
- [17] J. P. Delaroche, M. Girod, J. Libert, H. Goutte, S. Hilaire, S. Péru, N. Pillet, and G. F. Bertsch, *Phys. Rev. C* **81**, 014303 (2010).
- [18] Y. Fu, H. Mei, J. Xiang, Z. P. Li, J. M. Yao, and J. Meng, *Phys. Rev. C* **87**, 054305 (2013).
- [19] C. M. Bishop, *Pattern Recognition And Machine Learning*, 1st ed. (Springer-Verlag New York Inc., New York, 2006).
- [20] “See supplemental material at [url will be inserted by publisher] for technical details on conditioning the dataset and training the neural networks.” .
- [21] J. Yao, Y. Wu, and H. Zhai, [arXiv:1904.10692 \[cond-mat, physics:nucl-th, physics:physics\]](https://arxiv.org/abs/1904.10692) (2019), arXiv: 1904.10692.
- [22] F. Chollet, *Deep Learning with Python* (Manning Publications, Shelter Island, New York, 2017).
- [23] M. Abadi, P. Barham, J. Chen, Z. Chen, A. Davis, J. Dean, M. Devin, S. Ghemawat, G. Irving, M. Isard, M. Kudlur, J. Levenberg, R. Monga, S. Moore, D. G. Murray, B. Steiner, P. Tucker, V. Vasudevan, P. Warden, M. Wicke, Y. Yu, and X. Zheng, *Proceedings of the 12th USENIX Symposium on Operating Systems Design and Implementation*, 21 (2015).
- [24] S. J. Reddi, S. Kale, and S. Kumar, (2018).
- [25] D. P. Kingma and J. Ba, [arXiv:1412.6980 \[cs\]](https://arxiv.org/abs/1412.6980) (2014), arXiv: 1412.6980.
- [26] N. Wang, M. Liu, and X. Wu, *Phys. Rev. C* **81**, 044322 (2010).
- [27] S. Hilaire and M. Girod, *Eur. Phys. J. A* **33**, 237 (2007).
- [28] J. F. Berger, M. Girod, and D. Gogny, *Computer Physics Communications* **63**, 365 (1991).
- [29] W. Satuła, D. J. Dean, J. Gary, S. Mizutori, and W. Nazarewicz, *Physics Letters B* **407**, 103 (1997).
- [30] S. Goriely, M. Samyn, P.-H. Heenen, J. M. Pearson, and F. Tondeur, *Phys. Rev. C* **66**, 024326 (2002).
- [31] D. Regnier, N. Dubray, M. Verrière, and N. Schunck, *Computer Physics Communications* **225**, 180 (2018).
- [32] N. Chamel, S. Goriely, and J. M. Pearson, *Nuclear Physics A* **812**, 72 (2008).
- [33] S. Goriely, N. Chamel, and J. M. Pearson, *Phys. Rev. Lett.* **102**, 152503 (2009).
- [34] “Evaluated and Compiled Nuclear Structure Data,” .

[35] Y. Liu and X. Yao, *Neural Networks* **12**, 1399 (1999).